J. Fluid Mech. (2007), *vol.* 580, *pp.* 481–493.
doi:10.1017/S0022112007005757 Printed in the United Kingdom

Flow features resulting from shock wave impact on a cylindrical cavity

BERIC W. SKEWS[1] AND HARALD KLEINE[2]

[1]School of Mechanical, Industrial, and Aeronautical Engineering, University of the Witwatersrand, Johannesburg, 2050, South Africa

[2]School of Aerospace, Civil, and Mechanical Engineering, University of New South Wales, Australian Defence Force Academy, Canberra, ACT 2600, Australia

(Received 14 November 2006 and in revised form 25 January 2007)

The complex flow features that arise from the impact of a shock wave on a concave cavity are determined by means of high-speed video photography. Besides additional information on features that have previously been encountered in specific studies, such as those relating to shock wave reflection from a cylindrical wall and those associated with shock wave focusing, a number of new features become apparent when the interaction is studied over longer times using time-resolved imaging. The most notable of these new features occurs when two strong shear layers meet that have been generated earlier in the motion. Two jets can be formed, one facing forward and the other backward, with the first one folding back on itself. The shear layers themselves develop a Kelvin–Helmholtz instability which can be triggered by interaction with weak shear layers developed earlier in the motion. Movies are available with the online version of the paper.

1. Introduction

The study of shock wave interactions with a cavity has in the past almost exclusively dealt with shock focusing and the associated pressures that can be generated. The classic work is that of Sturtevant & Kulkarny (1976), who studied both plane and axisymmetric cases of a plane shock wave reflecting off a parabolic cavity. Izumi, Aso & Nishida (1994) extended this work in a comprehensive numerical and experimental study on shock focusing. All these focusing studies have used shallow parabolic reflectors, although Izumi *et al.* (1994) include one case with a cavity depth equal to half the aperture, similar to the proportions of the circular cavities used in the present investigation. Sturtevant & Kulkarny (1976) did not consider the early stage of incident wave reflection off the cavity surface but concentrated on the wave behaviour after the incident wave was fully reflected, and in particular studied the motion of the triple points. The locus of the triple-point motion is referred to as a shock–shock (Whitham 1957). Given the shallowness of the cavities used in these studies, the initial reflection at the entrance is regular, with the reflected shock diffracting around the entrance lip of the cavity. This shock will be referred to as a lip shock in the current work. Izumi *et al.* (1994) did not take their experiments much beyond the time when the shock–shocks from each side of the reflector meet and thus missed the flow features that are the main point of this paper. Shugaev & Shtemenko (1998) studied reflection of strong shocks ($M > 2$) from a variety of cavities, including small circular arc profiles. They identify the formation of a jet developing from the merging of the shear layers on the symmetry plane with a pair of associated vortices,

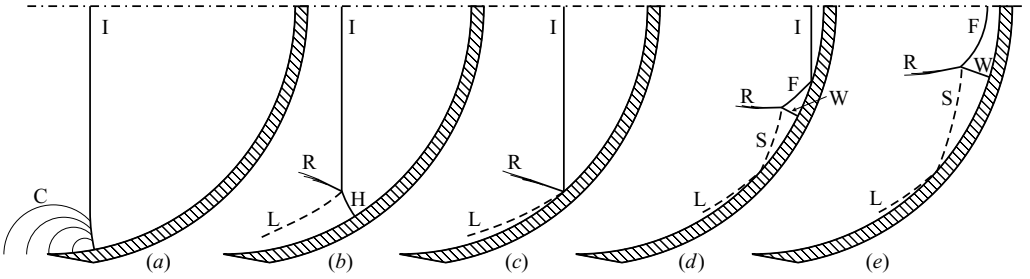

FIGURE 1. Evolution of the wave reflection pattern on a cylindrical surface.

to be described in this paper. Sturtevant & Kulkarny (1976) show one image of this mushroom-shaped jet, but do not elaborate on the features they observed. Their results were limited since the test section window was smaller than the cavity so that only part of the flow could be imaged.

In this work cylindrical cavities are investigated and although there are common features with the parabolic shape studies there are also significant differences, which have not previously been documented. The other main previous work of relevance is related to the wave reflection processes that occur when a plane shock wave strikes a cylindrical surface, as this generates the wave patterns which eventually meet on the focusing cavity's plane of symmetry. The various stages of the reflection process are shown schematically in figure 1. The evolution of the patterns shown in figure 1(b, c, d) has been treated by Ben-Dor (1992), but that study does not go to the stage where the incident wave is fully reflected from the rear of the cylinder nor does it deal with the very early stages if the cylindrical surface at the inlet is in the direction of shock motion. In this latter case no initial reflected shock is formed and the reflection consists of a continuous compression as successive compressive acoustic signals (C) are generated on the continuously steepening wall as shown in figure 1(a). This results in the incident shock curving forward so that its termination remains perpendicular to the wall. The compression waves C converge at the back of the curved portion of the wave causing the curvature to increase until a kink is formed in it and the compression develops into a short reflected shock (R) and a Mach reflection, MR, results. The triple point evolves from the kink; the location of the kink, however, does not coincide with the beginning of shock curvature, where the corner signal meets the incident wave, as will be demonstrated later.

Shadow photographs of this stage of the process show a reflected shock wave which appears to terminate in space since the gradients across the compression wave are too small to be imaged. If, however, the inlet lip of the cavity has a small but finite wall angle a reflected wave will form at the lip. A fully formed Mach reflection will thus be initiated from the moment the incident shock strikes the lip. This will be shown later to have important consequences for the subsequent motion. Although the triple point of the Mach reflection initially moves away from the wall (figure 1b) it will become an inverse Mach reflection as the incident wave penetrates the cavity and the wall angle steepens. The Mach stem (H) will reduce in length until the reflection becomes regular at the wall and the shear layer (L) is left stranded (figure 1c). The reflection then changes to regular reflection of a special form (figure 1d) which Ben-Dor (1992) has termed transitioned regular reflection (TRR). Examples of transition from MR to TRR for a circular arc and a concave double wedge have been presented by

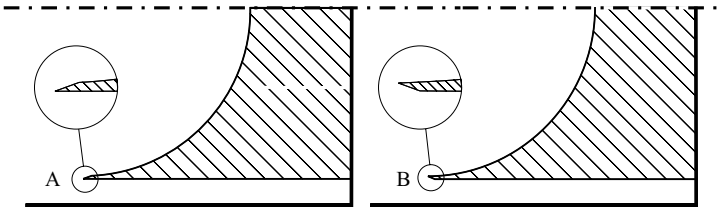

FIGURE 2. Test pieces.

Ben-Dor & Elperin (1991), together with an analysis of the wave configuration for the pseudo-steady case. At the confluence of the original reflected shock (R) and the new reflected shock (F) a third shock (W), connected to the wall, is established in order to balance the pressures. This will be referred to as the wall shock. A new shear layer (S) is formed from the new triple point. Upon reaching the bottom of the cavity, the incident wave (I) disappears and the reflected wave (F) changes into a converging cylindrical wave which becomes part of the focusing process on the axis of symmetry. The three-shock system (F, R, and W) and the shear layer (S), form the primary components of the subsequent flow. From a shock focusing perspective the gas dynamic focus is taken to be the point where the triple points from the two sides of the cavity impact on the plane of symmetry. The shear layers (S) from either side thus also meet at that point and their striking behaviour is a major point of discussion in this paper.

2. Apparatus

Tests were conducted in a simple shock tube having a test section 150 mm high and 75 mm wide. Nominal incident shock Mach numbers of 1.04, 1.22, and 1.33 were tested, with the shocks moving into ambient air at a pressure of 0.95 bar. A Shimadzu HPV-1 high-speed digital camera was used to obtain the video clips. Framing rates were varied between 125 k.f.p.s. and 1 M.f.p.s. (f.p.s. = frames per second) with exposure times per frame of between 250 ns and 1 μs; 102 frames are obtained for each test. Two test pieces, having profiles of 64 mm radius, shown in figure 2, were used. They are 130 mm high thereby leaving a 10 mm gap between the test piece and the top and bottom of the shock tube. The two profiles differed in that one (A) had a small inlet ramp on the inner surface. This ramp generated a weak shock wave followed by a weak expansion which served to identify the boundary of the flow influenced by the model surface, and which will be referred to as a corner signal or lip shock. It serves to define the boundary of influence of the cavity surface from either side. This feature had very interesting consequences, as described in § 6. The model with the external ramp (B) allows comparison with previous work on shock impact on a concave circular arc with a smooth entry. Owing to the leading edge not being perfectly sharp a very sensitive optical set-up can still detect, in some cases, the initial perturbation generated there. This has relevance to suggestions that transition from MR to TRR is related to the influence of this signal.

3. Primary features

Discussion of the flow pattern may be divided into two phases, corresponding to different aspects of the interaction as treated in the literature. The first is the reflection of the incident wave from the cylindrical surface as reviewed by Ben-Dor (1992), and

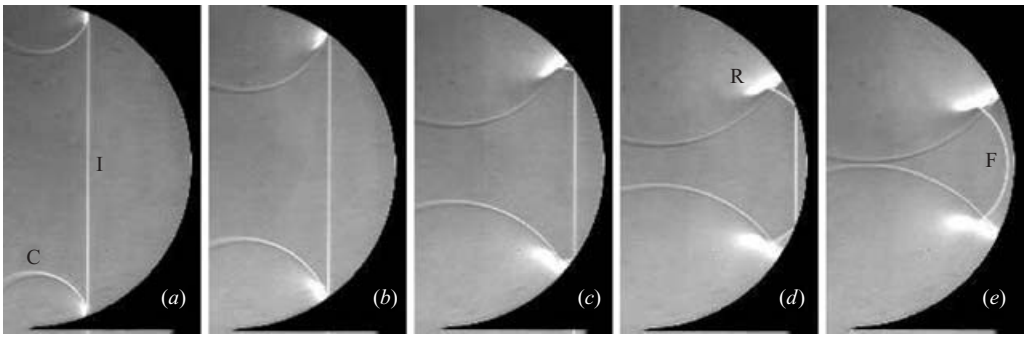

FIGURE 3. Schlieren images of a $M = 1.04$ shock; reflection phase on model A. Images (*a*)–(*c*) are 10 μs apart, Images (*c*)–(*e*) are 5 μs apart. Details of this evolution and that in figure 4 are given in movie 1, available with the online version of the paper.

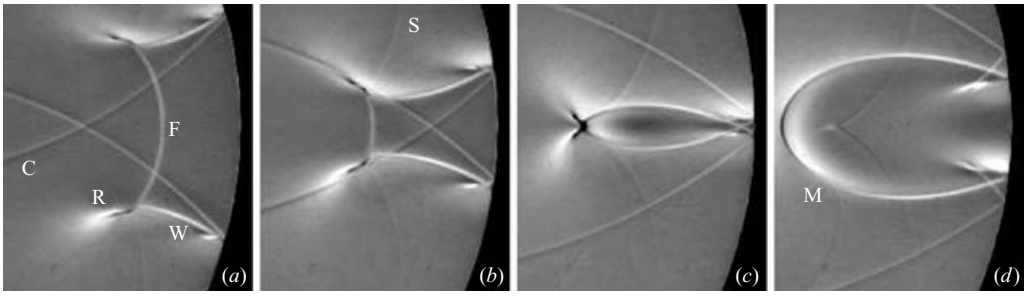

FIGURE 4. Schlieren images of a $M = 1.04$ shock; focusing phase, on model A. Images 20 μs apart.

the other is the focusing of the waves as treated by Sturtevant & Kulkarny (1976) and Izumi *et al.* (1994). Figure 3 shows a few frames from a test at a shock Mach number of 1.04 using model A, and corresponds closely to the schematic representation in figure 1.

Figure 4 shows the convergence of the waves R and F to a focus in frame (*c*). The shear layers, S, resulting from the confluence of the three-shock system between waves R, F, and W are discernible. Following the time of focus they meet and terminate as a slightly lighter spot behind the main reflected wave, M (figure 4*d*). This wave is generated from the crossing and merging of the two wall shocks (W). At this low Mach number no additional Mach reflections are formed, in contrast to the case of a parabolic reflector (Sturtevant & Kulkarny 1976), or to the case of stronger shock waves, as will be described later. In these two figures it can be seen how the lip shock initially terminates on the incident wave, then passes onto the reflected wave, and finally onto the wall shock, where it eventually meets the wall of the cavity and is reflected to form part of the reflection of the wall shock. Previous descriptions of the wall shock have indicated that it is plane and terminates perpendicular to the wall (Ben-Dor 1992). This is clearly not the case here, even at early times. It is curved, both while propagating inwards before the time of focus and after focus, and meets the wall at an angle, resulting in a regular reflection.

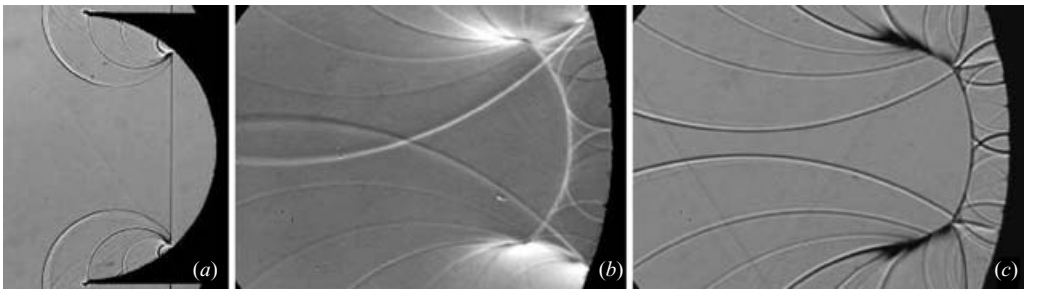

FIGURE 5. Images with wall disturbances using model A. (*a*) $M = 1.33$, shadowgraph. (*b*) $M = 1.06$, schlieren. (*c*) $M = 1.23$, shadowgraph. The propagation of these wavelets throughout the reflection process can be seen in movie 2.

4. Wall reflection

Although the reflection of a plane shock wave off a concave circular wall has received substantial attention (Ben-Dor 1992) additional information may be obtained from time-resolved imaging. One example is the development of the reflected wave, R. The transition from the compression wave of figure 1(*a*) to the Mach reflection of figure 1(*b*) and the further evolution of the reflected wave can be shown experimentally by placing minute perturbations on the surface of the cavity in order to generate very weak, essentially acoustic, waves in the flow. In the present case this is done by placing transverse strips of adhesive tape on the surface. The tape is 45 μm thick and 6 mm wide with strips placed at a pitch of 12 mm. Figure 5(*a*) shows the development of the perturbations at an early stage of the process. The first wavelet is a little stronger than the others because of the entrance geometry to the cavity and in fact consists of two waves – a weak shock as the incident wave encounters the entrance ramp closely followed by an expansion as the ramp joins the circular arc profile. These waves merge as they approach the incident shock. The important issue to note is that this wave intersects the incident wave further up the incident shock than where the triple point of the Mach reflection is initiated.

A clearer understanding of how the perturbations from the wall combine to form the reflected shock is obtained by changing the visualization optics to give a magnified image. An omnidirectional schlieren system with a circular cutoff is used for the weak wave case in figure 5(*b*), and a shadow system for the stronger wave in figure 5(*c*). These images clearly show how the perturbations arising from different parts of the cavity wall combine to form the reflected wave, and why it appears to terminate in space in a shadowgraph. Perturbations generated earlier in the cavity join the shock on one side whereas those generated later catch up on the other side. Studies of animations of these flows show that not all perturbations contribute to the formation of the reflected shock, as is evident in movie 2. In figure 5(*b*), for example, the first two signals run ahead of the reflected wave.

Using very weak perturbations of this type gives a method for determining when and where changes in wall shape have an influence on the flow field. Based on the length-scale criterion of Hornung, Oertel & Sandeman (1979), Ben-Dor & Takayama (1985) have suggested that the transition from MR to TRR will occur when the corner signal from the entrance to the cavity can no longer communicate with the reflection point. This implies that as long as the corner signal from the cavity inlet can reach the reflection point then Mach reflection remains possible. Ben-Dor & Takayama (1985) developed approximate transition criteria based on various assumptions regarding the

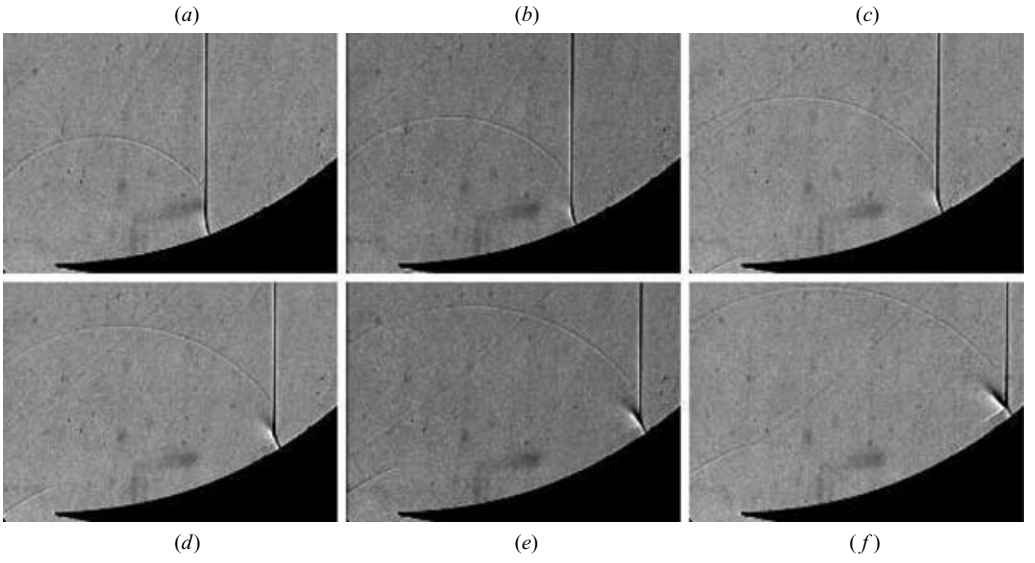

FIGURE 6. Shadow images of shock reflection transition from a reflected compression wave to a reflected shock wave. Model B. $M = 1.24$. Images are at 8 μs intervals. Movie 3 shows this development as well as that at the later stage given in figure 7.

path of the corner signal and obtained reasonable correlation. These criteria, however, are independent of the cavity radius, whereas experiments do show some influence, as shown by these same authors. They also do not account for perturbations generated elsewhere along the cavity profile, which are distributed in the flow, as evident in figure 5.

Time-resolved imaging is an ideal method to examine the position of the corner signal relative to the formation of the Mach stem and the transition to regular reflection. Figures 6 and 7 present images of the propagation of a Mach 1.24 shock taken with test piece B. The sensitivity of the visualization system is sufficient to record the very weak corner signal, which is made more obvious in the figures by adjusting the image contrast. Figure 6(*a*) shows the part of the shock below the corner signal intersection curving forward to meet the wall perpendicularly. The curvature decreases with time and a strong kink develops as the wall signals shown in figure 5 coalesce into a strong compression wave, which in Figure 6(*e*) develops into a shock, with the appearance of a slipstream from the newly formed MR. The corner signal also defines the limit to the region of influence of the wall. There is very little influence on the incident wave between the point where the corner signal contacts the incident shock and the kink and triple-point position.

Further evolution of the flow, for the same test, is shown in figure 7. In frame (*a*) the MR is well developed and the corner signal is ahead of the triple point and intersects the incident shock. However, frame (*b*) shows that the triple point has moved ahead and the corner signal is now intersecting the reflected shock. In frame (*c*) a slipstream is still evident, indicating the presence of Mach reflection, but the corner signal has been overtaken. In frame (*d*), which is the time of transition, the corner signal is left even further behind. Frames (*e*) and (*f*) show the TRR pattern. It is thus apparent that transition does not occur exactly when the corner signal can no longer affect the reflection point as originally suggested by Ben-Dor & Takayama (1985), although it occurs fairly close to this condition. The wall signals shown in figure 5 indicate that

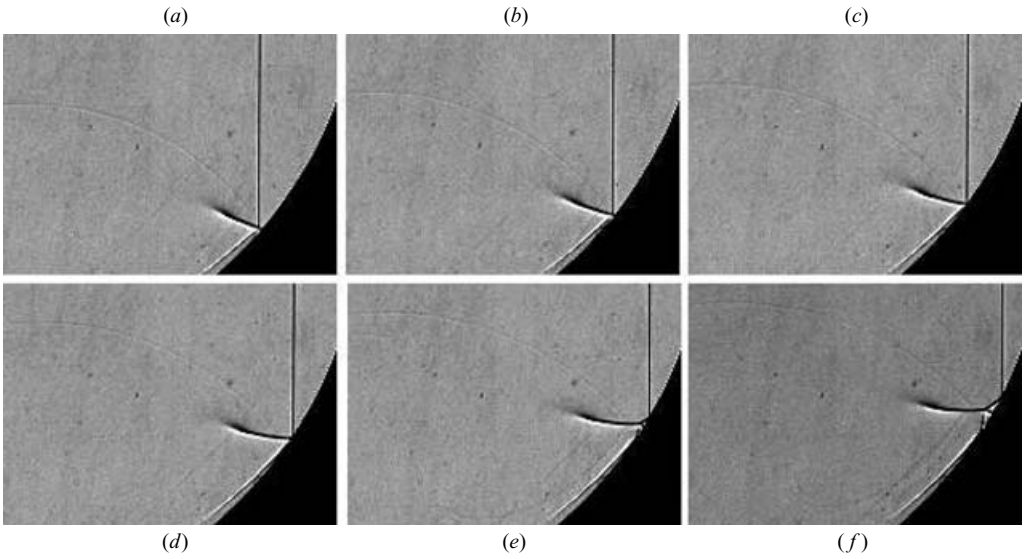

FIGURE 7. Shadow images of shock reflection transition from MR to TRR, showing the triple point outstripping the corner signal. Model B. $M = 1.24$. Images are at 4 μs intervals, and are for the same test as figure 6. Movie 3 shows the complete test.

the triple-point behaviour is, rather, influenced by the later shape of the wall and the perturbations coming off it. Thus if the wall curvature were to decrease along its length, rather than remaining constant, the Mach reflection would then be likely to, persist significantly beyond the corner signal position. The wall angle at transition for the current case is significantly different from transition criteria for pseudo-steady flows and indicates that flow unsteadiness can have a significant effect on conditions for transition. At even later times when the incident shock, I, has disappeared and the reflected shock, F, has been formed, the triple point is slowed down and eventually moves backwards towards the opening of the reflector, so that the corner signal can catch up with it again and finally overtake it. This can clearly be seen in figure 5(*b*).

5. Focus and post-focus wave behaviour

Whilst there is no sharp focal point of the wave system the term gas-dynamic focus will be used, as it is for parabolic cavities. This is taken to be when the shear layers from the TRR on either side of the cavity impact each other on the plane of symmetry. Figure 8 shows this situation for Mach numbers of 1.24 and 1.36 together with images taken a short time later. These can be compared with the $M = 1.04$ case given in figures 4(*c*) and 4(*d*). In figures 8(*a*) and (*c*) the triple points made up of the reflected shock, R, and the wall shock, W, from either side, and the focusing shock, F, meet (figure 1*e*), as wave F is reduced to zero. A short while later the main reflected wave, M, is formed from a combination of R and W. A smooth reflected wave is subsequently established with a shape similar to a truncated ellipse. The two shear layers and their terminal meeting point are left behind. In the $M = 1.04$ case (figure 4) the terminal point of the barely discernible shear layers appears as a small bright spot, which remains stationary for the rest of the observation period. In contrast to this, at higher Mach numbers (figure 8), a bifurcated flow pattern becomes apparent.

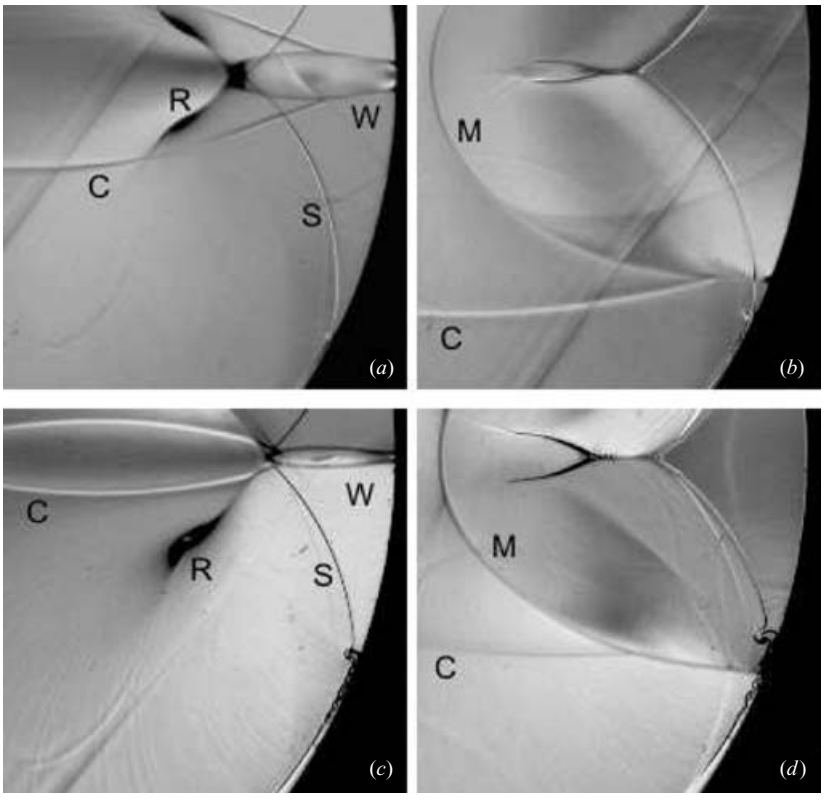

FIGURE 8. Schlieren images at focus and post focus. Model A. (a, b) $M = 1.24$, $\Delta t = 48\,\mu s$. (c, d) $M = 1.36$, $\Delta t = 50\,\mu s$. W – wall shock, R – reflected wave, S – TRR shear layer, M – main reflected wave, C – corner signal or lip shock.

The complex behaviour of these shear layers will be dealt with in the next section. Instabilities become evident where these layers meet the wall, and also in the earlier shear layer from the initial Mach reflection.

The main reflected wave, M, then moves towards the cavity entrance with an essentially cylindrical profile as shown in figure 9. This means that it meets the cavity wall at an angle, resulting in a regular reflection. A complex reflected wave, T, develops at the wall, made up of the successive compressions arising as the wall turns. Figure 9(*c*) is taken with the thin tape positioned on the cavity wall, so the way in which this reflected wave is formed can also be visualized. The weak wavelets that originally developed as the incident wave entered the cavity terminate on T as expected, whilst new wavelets develop when the main reflected shock passes over the edges of the tape. It is also to be noted that in all three of the images in figure 9 the position of the shear layers and their confluence has hardly moved from earlier positions. Furthermore the flow bifurcations noted in figure 8 for the stronger incident shocks have developed a more complex geometry with a bulbous-like tip.

6. The shear layer interactions

The first issue to address is what gives rise to the features associated with the meeting of the two opposing shear layers as seen in figure 9. Sturtevant & Kulkarny

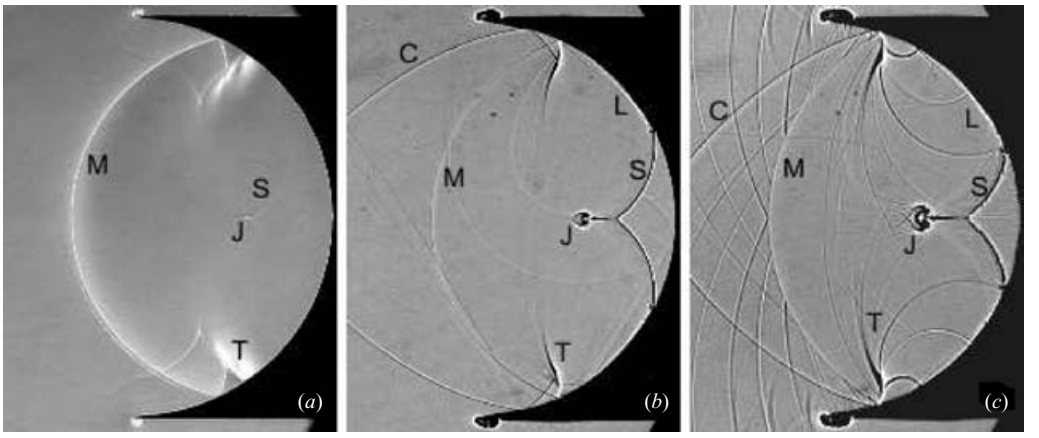

FIGURE 9. Main reflected wave emerging from the cavity (model A). (*a*) $M = 1.04$, schlieren, (*b*) $M = 1.22$, shadowgram, (*c*) $M = 1.33$, shadowgram, with surface steps. M – main reflected wave, J – jet, S – TRR shear layer, L – MR shear layer, C – corner signal or lip shock, T – re-reflected wave.

(1976) have shown that the initial shock–shock, which in this case is that due to the TRR, can cross on the axis of symmetry giving rise to a second pair of Mach reflections. The same applies in this case and the bifurcation pattern noted in figure 8 is established by the shear layers associated with these Mach reflections. The difference between the parabolic case and the current one is that the reflected waves of the Mach reflection get absorbed into the main smooth reflected wave (figures 4*d*, 8*b* and 8*d*) and the shock–shock ceases to exist. The shear layers thus also terminate. The main reflected shock develops from the two wall shocks. Figure 10 shows this process.

The shear layers do not move position significantly, but clearly the velocity gradient across them is substantial. At the point where these layers meet, a strong jet directed towards the cavity entrance is formed. This jet drives between the secondary shear layers causing them to roll up into a mushroom-shaped pair of vortices as shown in figure 11. It is also noted that the shear layers have developed Kelvin–Helmholtz (KH) instabilities. Interestingly, a small jet facing in the opposite direction is also developed at the confluence of the main shear layers, indicating the development of a stagnation point within the confluence. This jet has a much lower velocity. Major instabilities also appear on the main shear layer. Movie 4 shows the development of the features given in figures 10, 11, and 12.

The evolution of these instabilities is shown in figure 12 for test piece A. In the weaker shock wave case the instability starts at a particular and corresponding position on both the upper and lower shear layers, and at a later stage grows more uniformly on the remaining portions. For the strong wave case the instabilities grow rather uniformly along the length of the shear layer. The convolutions of the instability then continue to grow in time and finally show signs of breaking down into turbulence.

Strong vortices develop at the wall where the shear layers generated by the TRR meet with those generated by the earlier Mach reflection. The direction of rotation of this vortex indicates that the Mach reflection shear layer is pushing in under that from the TRR. These shear layers remain in close proximity to the wall and also show the development of KH instability.

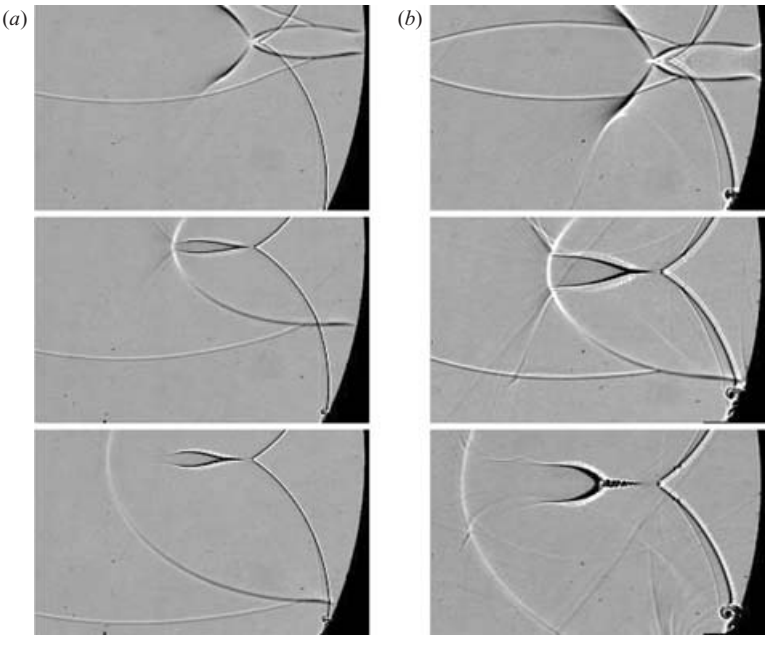

FIGURE 10. Post-focus development of new shear layers. Model A. (*a*) $M = 1.24$, time between frames = 24 μs. (*b*) $M = 1.35$, time between frames = 32 μs.

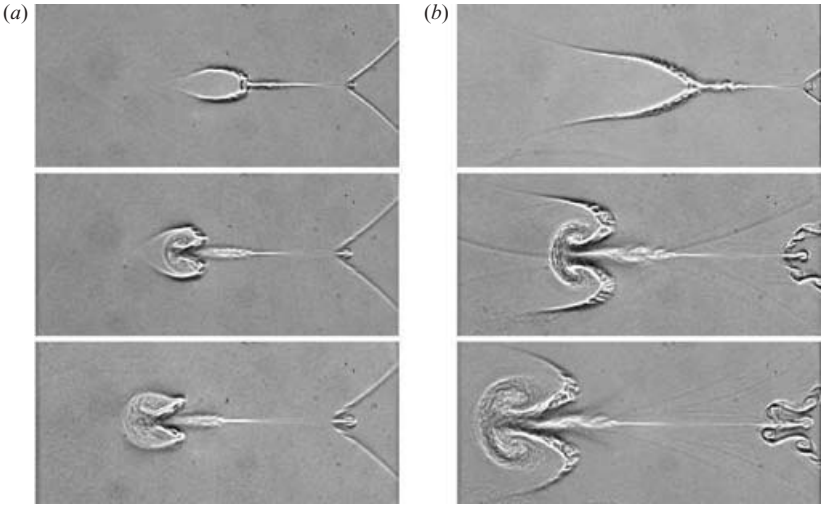

FIGURE 11. Jet development. Time between frames = 120 μs. (*a*) $M = 1.22$. (*b*) $M = 1.35$. Model A.

A number of tests at different shock Mach numbers showed the initiation of instability at specific points on both the top and bottom shear layers, which indicates that a flow-induced trigger exists. This type of instability onset is only observed for model A and not for model B. The trigger must thus arise from the leading-edge geometry. The reason is clarified in figure 13, together with a closer look at the growth of the instability. Frame (*a*) shows a pre-focus situation with the four main discontinuities (refer to figure 1*e*) of shocks F, W, and R, and shear layer S. A second,

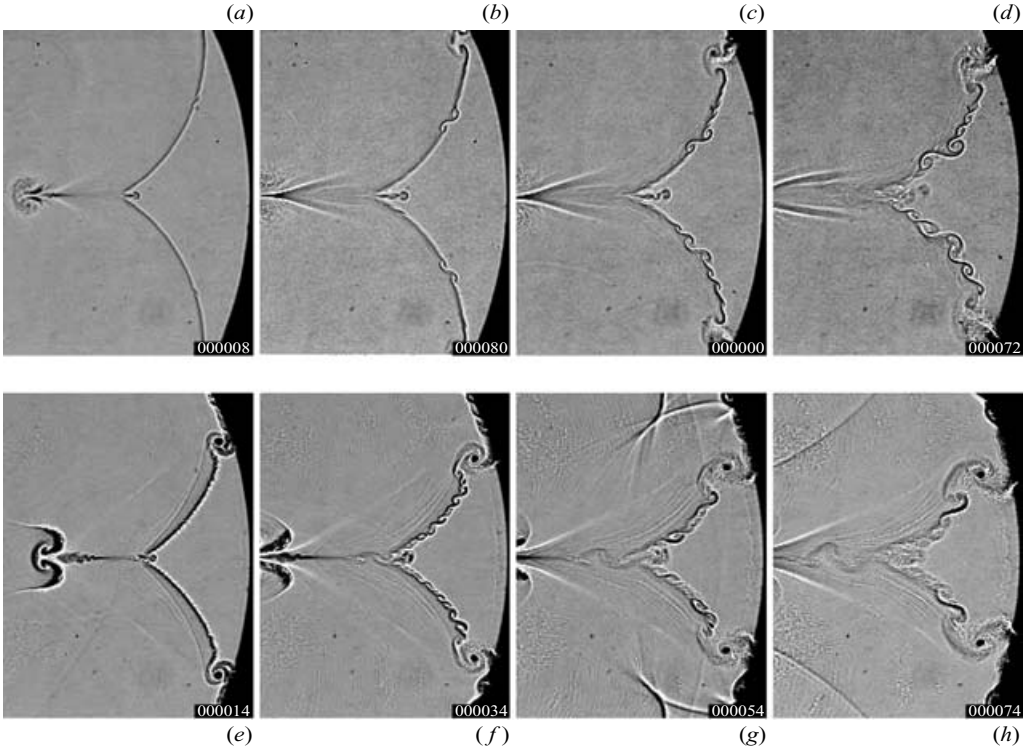

FIGURE 12. The development of Kelvin–Helmholtz instabilities. $M = 1.20$ (*a, b*) $M = 1.22$, (*c, d*) 720 μs between frames. $M = 1.38$, 200 μs between frames (*e–h*). Model A.

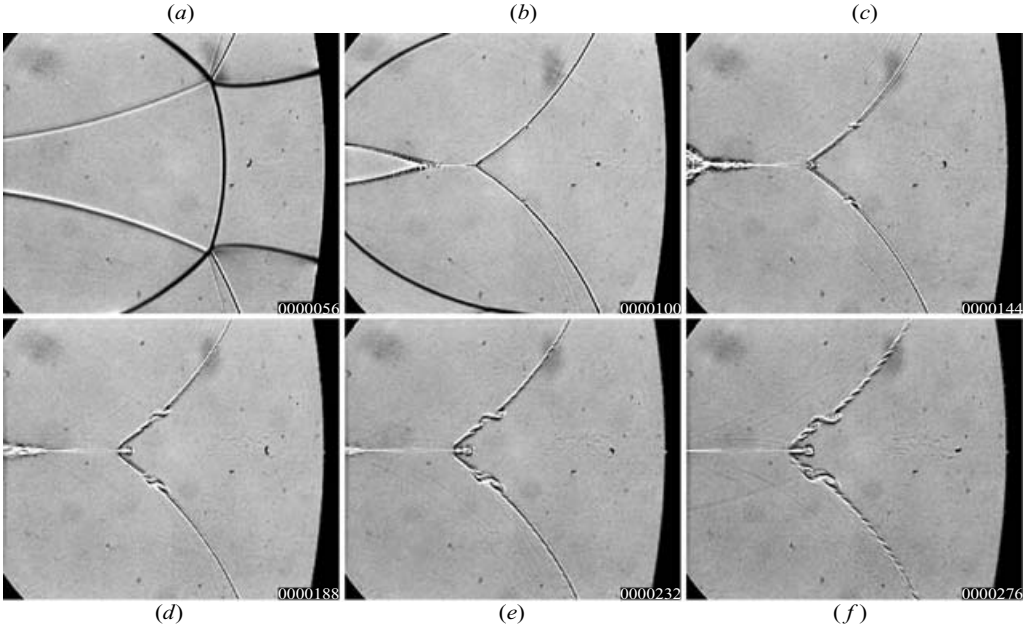

FIGURE 13. The initiation of the instability for model A at a Mach number of 1.34; 44 μs between frames.

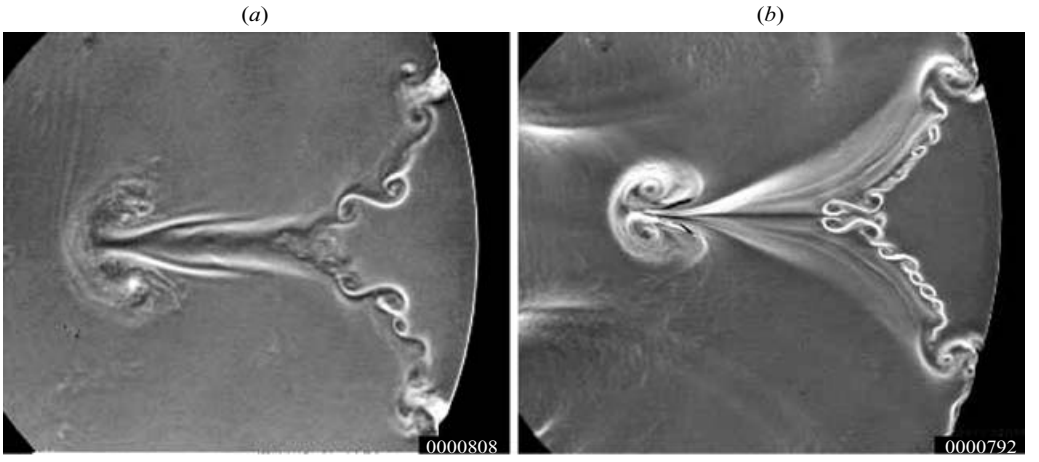

FIGURE 14. Schlieren images of late-stage shear flows for (*a*) $M = 1.21$ and (*b*) $M = 1.33$. Model A.

very weak shear layer develops where the lip shock intersects the reflected wave. Although this shear layer is barely discernible in the original images of later frames it is clearly the cause of the initiation of the instability. The mechanism is shown very clearly in movie 4. It is not known whether this phenomenon of a weak shear layer interacting with a stronger one causing the initiation of a Kelvin–Helmholtz instability has previously been noted. The reason why this effect is not observed for the slightly stronger shock case ($M = 1.38$) in figure 12 is that this weak shear layer, which is clearly visible in frame (*a*), does not intersect the main shear layer, but rather the subsequent jet. In the case of test piece B, where these weak shear layers are not present, the onset of the KH instability occurs later in time and less predictably, and with differences on the two sides of the cavity, indicating a more random perturbation causing the trigger.

Much of the visualization presented here has been conducted in the form of shadowgrams because of the clarity they give in features with sharp gradients. Schlieren imaging is also necessary in order to obtain an appreciation of shallower gradients. Figure 14 shows the additional features that become apparent. Particularly noticeable are the density gradients surrounding the jets. Detailed studies of these flows, probably by means of computer simulation, are planned.

7. Conclusions

A study of the nominally simple interaction of a shock wave with a cylindrical concave cavity has shown a wide variety of complex flow features. High-speed imaging proves to be a powerful tool in identifying these features. In particular the details of wave reflection off a curved wall, the development of the mechanisms leading to gas-dynamic focusing, the development of jets, and the initiation and growth of Kelvin–Helmholtz instabilities on shear layers are identified. Only a limited range of variables have been explored in this work and follow-up research is planned.

B.W.S. gratefully acknowledges the award of an ADFA Rector's Visiting Fellowship in order to conduct this research.

REFERENCES

Ben-Dor, G. 1992 *Shock Wave Reflection Phenomena*. Springer.

Ben-Dor, G. & Elperin, T. 1991 Analysis of the wave configuration resulting from the termination of an inverse Mach reflection. *Shock Waves* **1**, 237–241.

Ben-Dor, G. & Takayama, K. 1985 Analytical prediction of the transition from Mach to regular reflection over cylindrical concave wedges. *J. Fluid Mech.* **158**, 365–380.

Hornung, H.G., Oertel, H. & Sandeman, R. J. 1979 Transition to Mach reflection of shock waves in steady and pseudo-steady flows with and without relaxation. *J. Fluid Mech.* **90**, 541–560.

Izumi, K., Aso, S. & Nishida, M. 1994 Experimental and computational studies focusing processes of shock waves reflected from parabolic reflectors. *Shock Waves* **3**, 213–222.

Shugaev, F. V. & Shtemenko, L. S. 1998 *Propagation and Reflection of Shock Waves*. World Scientific.

Sturtevant, B. & Kulkarny, V. A. 1976 The focusing of weak shock waves. *J. Fluid Mech.* **73**, 651–671.

Whitham, G. B. 1957 A new approach to problems of shock dynamics. Part 1. Two-dimensional problems. *J. Fluid Mech.* **2**, 145–171.